Predictor Design for Connected Cruise Control Subject to Packet Loss

Tamás G. Molnár[*], **Wubing B. Qin**[**], **Tamás Insperger**[*], and **Gábor Orosz**[**]

[*] *Department of Applied Mechanics, Budapest University of Technology and Economics, Budapest H-1111, Hungary (e-mail: molnar@mm.bme.hu, insperger@mm.bme.hu)*
[**] *Department of Mechanical Engineering, University of Michigan, Ann Arbor, MI 48109, USA (e-mail: wubing@umich.edu, orosz@umich.edu)*

Abstract: In this work connected cruise control with digital controllers is investigated for a vehicular string on a single lane. The longitudinal control of each vehicle is based on the information broadcast by other vehicles via wireless communication. We demonstrate that intermittencies and packet loss introduce time-dependent time delays in the control loop that may destabilize the system. We analyze the plant and string stability and construct predictors to attenuate the destabilizing effects of the imperfections in the communication.

Keywords: connected vehicles, digital control, stability, predictor

1. INTRODUCTION

Arising technologies in vehicle-to-vehicles (V2V) communications have a large potential to improve safety and mobility of vehicular traffic; see Caveney (2010); Zhang and Orosz (2015). The fact that human drivers have large reaction times ($0.5 - 1$ [s]) and that they are only able to monitor the motion of the vehicle immediately in front makes it difficult to attenuate congestion waves traveling upstream. This so-called string instability was introduced in Swaroop and Hedrick (1996) and it typically leads to the formation of stop-and-go traffic jams as shown in Orosz et al. (2010).

Wireless vehicle-to-vehicle (V2V) communication may be used to obtain information beyond the line of sight which can be beneficial for attenuating congestion waves. For example, a platoon of vehicles equipped with radars can monitor the motion of a designated platoon leader via communication, which is referred as cooperative adaptive cruise control (CACC); see Rajamani and Shladover (2001); van Arem et al. (2006); Öncü et al. (2014). However, this architecture is not practical for real traffic situations since the probability that multiple radar equipped vehicles travel next to each other is very small, and all vehicles talking to a leader is not possible due to the limited range of V2V communication. Thus, the concept of connected cruise control (CCC) was established in Orosz (2014); Ge and Orosz (2014) which uses all available V2V signals when inserted into a flow of human-driven vehicles. CCC may be used to support the human driver, to supplement sensory information, or to control the longitudinal motion of vehicle.

However, V2V communication is intermittent: the sampling period 100 [ms] is used for dedicated short range communication (DSRC) devices. This introduces time varying time delays into the control loops as explained in Qin and Orosz (2013). Moreover, the delays may increase due to packet drops. In this paper we investigate the dynamics of vehicular strings when assuming deterministic packet drop scenarios. Moreover, we design predictors to compensate the detrimental effect of the delays. We demonstrate that with the predictors one may design controllers that are robust against packet drops.

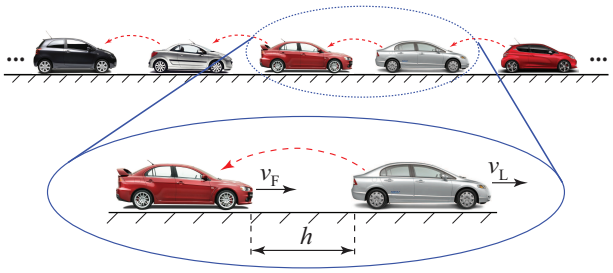

Fig. 1. Connected vehicles on a single lane. The configuration above can be viewed as the concatenation of the leader-follower pattern shown below. The red dashed arrows indicate V2V communication.

2. MATHEMATICAL MODEL

We consider a string of connected vehicles on a single lane as shown in Fig. 1. We assume that the motion of each vehicle is controlled based on the data sent by the vehicle immediately ahead. When considering identical vehicles, one may characterize the dynamics of the vehicular string by focusing on the leader-follower configuration shown at the bottom of Fig. 1. The headway h, the leader's velocity v_L and the follower's velocity v_F satisfy the kinematic constraint

$$\dot{h}(t) = v_L(t) - v_F(t)\,. \tag{1}$$

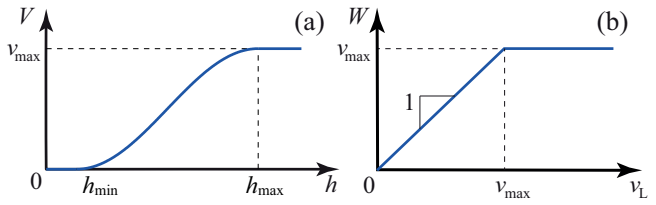

Fig. 2. (a) The desired velocity (3,4) as a function of the headway. (b) The saturation function (6).

Here we neglect rolling resistance, air drag and elevation for the sake of simplicity. Thus, the follower's acceleration is assigned by the control input, i.e.,

$$\dot{v}_{\rm F}(t) = a_{\rm des}(t)\,. \tag{2}$$

The follower's desired velocity $V(h)$ can be designed as a function of the headway according to the range policy

$$V(h) = \begin{cases} 0 & \text{if } h \le h_{\min}\,, \\ F(h) & \text{if } h_{\min} < h < h_{\max}\,, \\ v_{\max} & \text{if } h \ge h_{\max}\,. \end{cases} \tag{3}$$

That is, if the headway drops below a lower limit $h_{\min}$, the follower intends to stop. For larger headway, the desired velocity increases monotonously according to the function $F(h)$. If the headway exceeds an upper limit $h_{\max}$, the vehicle shall travel with the maximum velocity $v_{\max}$ allowed by traffic regulations. Note that $F(h_{\min}) = 0$ and $F(h_{\max}) = v_{\max}$. To achieve smooth acceleration, we also require $F'(h_{\min}) = F'(h_{\max}) = 0$, and here we choose

$$F(h) = \frac{v_{\max}}{2}\left[1 - \cos\left(\pi \frac{h - h_{\min}}{h_{\max} - h_{\min}}\right)\right]\,. \tag{4}$$

The range policy (3,4) is shown in Fig. 2(a), while other choices on $V(h)$ can be found in Orosz (2014).

Here we propose the proportional-velocity (PV) controller

$$a_{\rm des}(t) = \alpha\left[V(h(t)) - v_{\rm F}(t)\right] + \beta\left[W\big(v_{\rm L}(t)\big) - v_{\rm F}(t)\right], \tag{5}$$

where parameters α and β denote the control gains. The saturation function $W(v_{\rm L})$ describes the switching between CCC mode ($v_{\rm L} \le v_{\max}$) and normal cruise control mode ($v_{\rm L} > v_{\max}$) such that

$$W(v_{\rm L}) = \begin{cases} v_{\rm L} & \text{if} \quad v_{\rm L} \le v_{\max}\,, \\ v_{\max} & \text{if} \quad v_{\rm L} > v_{\max}\,, \end{cases} \tag{6}$$

which is plotted in Fig. 2(b). Note that other control strategies also exist; see Orosz et al. (2010) for more details. When $v_{\rm L} \le v_{\max}$, the system (1,2) with control law (5) possesses the uniform flow equilibrium

$$V(h^*) = v_{\rm F}^* = v_{\rm L}^*\,, \tag{7}$$

where the vehicles travel with the same constant velocity while keeping a constant headway h^*.

3. DIGITAL CONTROL

Here we assume that the clocks of the leader and the follower are synchronized. Given that a digital controller is implemented with sampling period Δt, the leader's velocity $v_{\rm L}$, the follower's velocity $v_{\rm F}$, and the headway h are sampled at discrete time instants $t_k = k\Delta t$. Since these data are not readily available at time instant t_k due to the processing delay, the controller uses the data obtained at the previous sampling instant t_{k-1}. The corresponding control input is held constant by a zero-order-hold (ZOH)

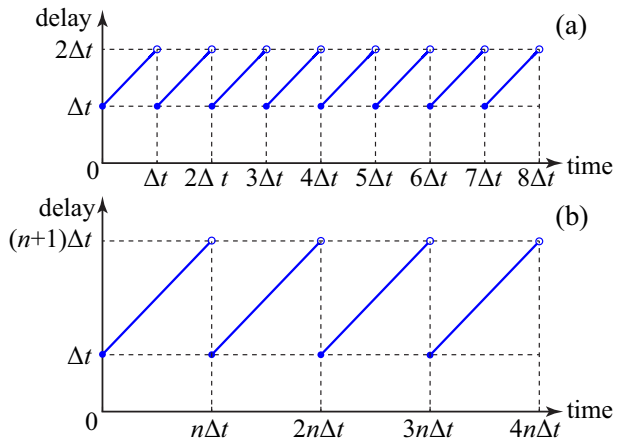

Fig. 3. The delay variation of the system: (a) with reliable communication (no packet drops), (b) when every n-th packet is received.

in the time interval $[t_k, t_{k+1})$. Accordingly, the control law can be written as

$$\dot{v}_{\rm F}(t) = a_{\rm des}(t_{k-1})\,, \quad t \in [t_k, t_{k+1}). \tag{8}$$

Note that the ZOH introduces a time varying time delay that increases linearly from Δt to $2\Delta t$ during each period as shown in Fig. 3(a). For dedicated short range communication (DSRC) devices, the typical sampling period is $\Delta t = 0.1$ [s].

Equations (5,8) yield a continuous-time nonlinear system with piecewise constant input. According to Stépán (2001), the stability of such systems can be analyzed using a discrete map. By solving the system in the time interval $t \in [t_k, t_{k+1})$ with the initial conditions at t_k, one can get the discrete-time map

$$\begin{aligned} \begin{bmatrix} h(k+1) \\ v_{\rm F}(k+1) \end{bmatrix} &= \begin{bmatrix} 1 & -\Delta t \\ 0 & 1 \end{bmatrix} \begin{bmatrix} h(k) \\ v_{\rm F}(k) \end{bmatrix} + \begin{bmatrix} \int_{t_k}^{t_{k+1}} v_{\rm L}(t){\rm d}t \\ 0 \end{bmatrix} \\ &+ \begin{bmatrix} 0 & \frac{1}{2}(\alpha+\beta)\Delta t^2 \\ 0 & -(\alpha+\beta)\Delta t \end{bmatrix} \begin{bmatrix} h(k-1) \\ v_{\rm F}(k-1) \end{bmatrix} \\ &+ \begin{bmatrix} -\frac{1}{2}\alpha\Delta t^2 \\ \alpha\Delta t \end{bmatrix} V\left(h(k-1)\right) + \begin{bmatrix} -\frac{1}{2}\beta\Delta t^2 \\ \beta\Delta t \end{bmatrix} W\big(v_{\rm L}(k-1)\big)\,, \end{aligned} \tag{9}$$

where we used the notation $h(k) = h(t_k)$, $v_{\rm F}(k) = v_{\rm F}(t_k)$, $v_{\rm L}(k) = v_{\rm L}(t_k)$.

In order to carry out the linear stability analysis, one can consider small fluctuations in the leader's velocity about a constant value, i.e., $v_{\rm L}(t) = v_{\rm L}^* + \tilde{v}_{\rm L}(t)$, and assume small variations around the equilibrium (7), i.e., $h(t) = h^* + \tilde{h}(t)$, $v_{\rm F}(t) = v_{\rm F}^* + \tilde{v}_{\rm F}(t)$. Thus, by linearizing (9) one obtains

$$\begin{aligned} \begin{bmatrix} \tilde{h}(k+1) \\ \tilde{v}_{\rm F}(k+1) \end{bmatrix} &= \begin{bmatrix} 1 & -\Delta t \\ 0 & 1 \end{bmatrix} \begin{bmatrix} \tilde{h}(k) \\ \tilde{v}_{\rm F}(k) \end{bmatrix} + \begin{bmatrix} \int_{t_k}^{t_{k+1}} \tilde{v}_{\rm L}(t){\rm d}t \\ 0 \end{bmatrix} \\ &+ \begin{bmatrix} -\frac{1}{2}\alpha V'(h^*)\Delta t^2 & \frac{1}{2}(\alpha+\beta)\Delta t^2 \\ \alpha V'(h^*)\Delta t & -(\alpha+\beta)\Delta t \end{bmatrix} \begin{bmatrix} \tilde{h}(k-1) \\ \tilde{v}_{\rm F}(k-1) \end{bmatrix} \\ &+ \begin{bmatrix} -\frac{1}{2}\beta\Delta t^2 \\ \beta\Delta t \end{bmatrix} \tilde{v}_{\rm L}(k-1)\,, \end{aligned} \tag{10}$$

where

$$V'(h^*) = \begin{cases} 0 & \text{if } h^* \le h_{\min} \ , \\ F'(h^*) & \text{if } h_{\min} < h^* < h_{\max} \ , \\ 0 & \text{if } h^* \ge h_{\max} \ , \end{cases} \tag{11}$$

cf. (3).

According to Fourier's theory, any absolutely integrable function can be written as an infinite sum of harmonic functions. Thus, we assume sinusoidal fluctuations in leader's velocity, i.e.,

$$\tilde{v}_{\rm L}(t) = v_{\rm L}^{\rm amp} \sin(\omega t) \ . \tag{12}$$

By defining the state, the input, and the output as

$$x(k) = \begin{bmatrix} \tilde{h}(k) \\ \tilde{v}_{\rm F}(k) \end{bmatrix}, \quad u(k) = \tilde{v}_{\rm L}(k), \quad y(k) = \tilde{v}_{\rm F}(k), \tag{13}$$

system (10) subject to (12) becomes

$$\begin{aligned} x(k+1) &= \mathbf{a}_0 \, x(k) + \mathbf{a}_1 \, x(k-1) \\ &\quad + \mathbf{b}_0 \, u(k) + \mathbf{b}_1 \, u(k-1) + \mathbf{b}_2 \, u(k-2) \ , \\ y(k) &= \mathbf{c} \, x(k) \ , \end{aligned} \tag{14}$$

where

$$\mathbf{a}_0 = \begin{bmatrix} 1 & -\Delta t \\ 0 & 1 \end{bmatrix}, \ \mathbf{a}_1 = \begin{bmatrix} -\frac{1}{2}\alpha V'(h^*)\Delta t^2 & \frac{1}{2}(\alpha+\beta)\Delta t^2 \\ \alpha V'(h^*)\Delta t & -(\alpha+\beta)\Delta t \end{bmatrix},$$

$$\mathbf{b}_0 = \begin{bmatrix} \beta_1 \\ 0 \end{bmatrix}, \ \mathbf{b}_1 = \begin{bmatrix} -\frac{1}{2}\beta\Delta t^2 \\ \beta \Delta t \end{bmatrix}, \ \mathbf{b}_2 = \begin{bmatrix} \beta_2 \\ 0 \end{bmatrix}, \ \mathbf{c} = [0 \ 1], \tag{15}$$

and

$$\beta_1 = \frac{\cos(2\omega\Delta t) - \cos(3\omega\Delta t)}{\omega \sin(2\omega\Delta t)}, \ \ \beta_2 = \frac{\cos(\omega\Delta t) - 1}{\omega \sin(2\omega\Delta t)}. \tag{16}$$

Here we exploited that the integral in (10) can be written into the form

$$\int_{t_k}^{t_{k+1}} \tilde{v}_{\rm L}(t) {\rm d}t = \beta_1 \tilde{v}_{\rm L}(t_k) + \beta_2 \tilde{v}_{\rm L}(t_{k-2}) \ . \tag{17}$$

By defining the augmented state

$$X(k) = \begin{bmatrix} x(k) \\ x(k-1) \end{bmatrix}, \tag{18}$$

equation (14) can be re-written as

$$\begin{aligned} X(k+1) &= \mathbf{A}_1 X(k) + \mathbf{B}_0 u(k) + \mathbf{B}_1 u(k-1) + \mathbf{B}_2 u(k-2), \\ y(k) &= \mathbf{C} X(k) \, , \end{aligned} \tag{19}$$

with matrices

$$\mathbf{A}_1 = \begin{bmatrix} \mathbf{a}_0 & \mathbf{a}_1 \\ \mathbf{I} & \mathbf{0} \end{bmatrix}, \ \mathbf{B}_0 = \begin{bmatrix} \mathbf{b}_0 \\ \mathbf{o} \end{bmatrix}, \ \mathbf{B}_1 = \begin{bmatrix} \mathbf{b}_1 \\ \mathbf{o} \end{bmatrix}, \ \mathbf{B}_2 = \begin{bmatrix} \mathbf{b}_2 \\ \mathbf{o} \end{bmatrix},$$
$$\mathbf{C} = \begin{bmatrix} \mathbf{c} \ \mathbf{o}^{\rm T} \end{bmatrix}. \tag{20}$$

Here, $\mathbf{0} \in \mathbb{R}^{2\times 2}$ and $\mathbf{I} \in \mathbb{R}^{2\times 2}$ denote the zero and identity matrices, respectively, while $\mathbf{o} \in \mathbb{R}^2$ denotes the zero vector, and T stands for transpose.

4. PLANT AND STRING STABILITY ANALYSIS

When designing a controller for a CCC vehicle, plant and string stability must be guaranteed. Therefore, stability analysis of (19) will be conducted in this section, which follows the methods presented in Qin and Orosz (2013). Plant stability means that the follower is able to approach leader's constant velocity $v_{\rm L}^*$. Thus, we assume $\tilde{v}_{\rm L}(t) \equiv 0$ in (19) that yields the linear map

$$X(k+1) = \mathbf{A}_1 X(k) \ . \tag{21}$$

To ensure plant stability, all eigenvalues of $\mathbf{A}_1$ given by the characteristic equation

$$\det(z\mathbf{I} - \mathbf{A}_1) = 0 \tag{22}$$

must lie within the unit circle in the complex plane. There are three critical situations when plant stability is lost: $z = 1$, $z = -1$, and $z = {\rm e}^{\pm {\rm i}\theta}$ where ${\rm i}^2 = -1$ and $\theta \in (0, \pi)$. When $z = 1$ and $z = -1$, (22) yields the plant stability boundaries

$$\alpha = 0 \ , \tag{23}$$

$$\alpha = -\frac{2}{\Delta t} - \beta \ , \tag{24}$$

respectively. For $z = {\rm e}^{\pm {\rm i}\theta}$, the real and imaginary parts need to be separated to obtain the plant stability boundary that is parameterized by $\theta \in (0, \pi)$.

String stability refers to the follower's capability of attenuating fluctuations in the leader's velocity, which is needed to avoid the formation of traffic jams. This is characterized by the amplification ratio from input to output. By applying Z transform to (19), one can get the transfer function

$$\Gamma(z) = \mathbf{C}(z\mathbf{I} - \mathbf{A}_1)^{-1} \left(\mathbf{B}_2 z^{-2} + \mathbf{B}_1 z^{-1} + \mathbf{B}_0 \right) \ , \tag{25}$$

yielding the magnitude ratio

$$M(\omega) = \left| \Gamma \left({\rm e}^{{\rm i}\omega\Delta t} \right) \right| . \tag{26}$$

Hence, the necessary and sufficient condition for string stability is

$$M(\omega) < 1, \quad \forall \omega > 0. \tag{27}$$

Considering $\omega = \omega_{\rm cr}$ at the boundary of string stability, three different cases are possible: $\omega_{\rm cr} = 0$, $\omega_{\rm cr} = (2k+1)\pi/\Delta t$ with $k = 0, 1, 2, ...$, and when $\omega_{\rm cr}$ is not equal to either of these. Since $M(0) = 1$ and $M'(0) = {\rm d}M/{\rm d}\omega \, (0) = 0$ always hold, at $\omega_{\rm cr} = 0$ the string stability boundary is given by $M''(0) = 0$, which yields

$$\alpha = 0 \ , \tag{28}$$

$$\alpha = \frac{2\left(V'(h^*) - \beta\right)}{1 - \frac{1}{6}\left(V'(h^*)\right)^2 \Delta t^2} \ . \tag{29}$$

At $\omega_{\rm cr} = (2k+1)\pi/\Delta t$ condition $M(\omega_{\rm cr}) = 1$ gives

$$\beta = \frac{1}{2\alpha + 4/\Delta t} \left[\left(\frac{V'(h^*)^2 \Delta t^2}{(2k+1)^2 \pi^2} - 1 \right) \alpha^2 - \frac{4}{\Delta t}\alpha - \frac{4}{\Delta t^2} \right]. \tag{30}$$

For $\omega_{\rm cr} > 0$, $\omega_{\rm cr} \neq (2k+1)\pi/\Delta t$ equations $M(\omega_{\rm cr}) = 1$ and $M'(\omega_{\rm cr}) = 0$ need to be solved numerically in order to obtain the string stability boundaries that are parameterized by $\omega_{\rm cr}$.

Fig. 4 shows the stability diagram in the (β, α)-plane for $h_{\min} = 5$ [m], $h_{\max} = 35$ [m], $v_{\max} = 30$ [m/s], $h^* = 20$ [m], and $v_{\rm L}^* = v_{\rm F}^* = 15$ [m/s], which will be kept the same through the paper. The dashed red line corresponds to the plant stability boundary for $z = 1$, while the solid red curve is the plant stability boundary for $z = {\rm e}^{{\rm i}\theta}$. Similarly, the dashed and dotted blue lines correspond to string stability boundaries for $\omega_{\rm cr} = 0$ and $\omega_{\rm cr} = \pi/\Delta t$, respectively, while the solid blue curve corresponds to the string stability boundary for $\omega_{\rm cr} > 0$. The plant and string stable regions are shaded with light and dark gray, respectively, and the gains (β, α) should be chosen from their intersection, where the system is both plant and string stable. However, this region shrinks as Δt is increased. At the critical case

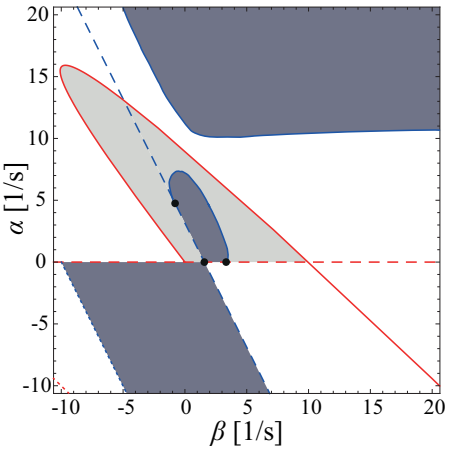

Fig. 4. Stability diagram in the (β, α)-plane when $\Delta t = 0.1$ [s]. Red and blue curves correspond to changes in plant and string stability, respectively. The light gray region is plant stable, the dark gray regions are string stable.

$$\Delta t_{\text{crit}} = \frac{1}{3V'(h^*)} \,, \tag{31}$$

the three intersection points marked by black dots coincide, leading to the disappearance of the string stable region. (The location of these points can be calculated from the higher derivatives of $M(\omega)$, and thus (31) can be proven.) In our case, $V'(h^*) = \pi/2$ [1/s] which yields $\Delta t_{\text{crit}} = 0.212$ [s]. We remark that (31) matches the result in Zhang and Orosz (2015) for the continuous time-delay approximation using the average delay $\bar{\tau} = 3/2\,\Delta t$, cf. Fig. 3(a).

5. EFFECTS OF PACKET LOSSES

Since wireless communication is not always reliable, there may be packet losses in vehicle-to-vehicle communication. In this case the controller relies on the last available measurement data, leading to an increase of the time delay. In this section, we assume that the follower's velocity is measured on board and available at each time instant, i.e., only the leader's velocity and the headway are influenced by packet loss. Moreover, we restrict ourselves to cases where packet losses occur deterministically. We remark that considering stochastic packet losses is more realistic, as discussed in Verriest and Michiels (2009) and in Qin et al. (2014, 2015). Considering $\tau(k)-1$ consecutive packet losses, the control law becomes

$$\begin{aligned} \dot{v}_{\text{F}}(t) = {} & \alpha \left[V\left(h(t_{k-\tau(k)})\right) - v_{\text{F}}(t_{k-1}) \right] \\ & + \beta \left[W\left(v_{\text{L}}(t_{k-\tau(k)})\right) - v_{\text{F}}(t_{k-1}) \right] \,, \quad t \in [t_k, t_{k+1}) \,. \end{aligned} \tag{32}$$

Note that $\tau(k) = 1$ yields the no packet loss case (5,8).

Similar to the no packet loss case, by solving (1,32) subject to the sinusoidal fluctuations (12) in the leader's velocity, with initial condition at t_k, one can obtain the linearized discrete-time system

$$\begin{aligned} x(k+1) = {} & \mathbf{a}_0\, x(k) + \tilde{\mathbf{a}}_1\, x(k-1) + \tilde{\mathbf{a}}_\tau\, x(k-\tau(k)) \\ & + \mathbf{b}_0\, u(k) + \mathbf{b}_2\, u(k-2) + \tilde{\mathbf{b}}_\tau\, u(k-\tau(k)) \,, \\ y(k) = {} & \mathbf{c}\, x(k) \,, \end{aligned} \tag{33}$$

cf. (13,14,15), where $\mathbf{a}_0,\ \mathbf{b}_0,\ \mathbf{b}_2,\ \mathbf{c}$ are defined in (15) and

$$\begin{aligned} \tilde{\mathbf{a}}_1 &= \begin{bmatrix} 0 & \frac{1}{2}(\alpha+\beta)\Delta t^2 \\ 0 & -(\alpha+\beta)\Delta t \end{bmatrix}, \ \tilde{\mathbf{a}}_\tau = \begin{bmatrix} -\frac{1}{2}\alpha V'(h^*)\Delta t^2 & 0 \\ \alpha V'(h^*)\Delta t & 0 \end{bmatrix}, \\ \tilde{\mathbf{b}}_\tau &= \mathbf{b}_1. \end{aligned} \tag{34}$$

Note that $\tilde{\mathbf{a}}_1 + \tilde{\mathbf{a}}_\tau = \mathbf{a}_1$ that is given in (15). The corresponding augmented state-space representation becomes

$$\begin{aligned} X(k+1) = {} & \mathbf{A}_{\tau(k)} X(k) \\ & + \mathbf{B}_0 u(k) + \mathbf{B}_2 u(k-2) + \mathbf{B}_\tau u(k-\tau(k)), \\ y(k) = {} & \mathbf{C} X(k) \,, \end{aligned} \tag{35}$$

where

$$\begin{aligned} X(k) &= \begin{bmatrix} x(k) \\ x(k-1) \\ \vdots \\ x\big(k-\tau(k)\big) \end{bmatrix}, \ \mathbf{A}_{\tau(k)} = \begin{bmatrix} \mathbf{a}_0 & \tilde{\mathbf{a}}_1 & \mathbf{0} & \cdots & \mathbf{0} & \tilde{\mathbf{a}}_\tau \\ \mathbf{I} & \mathbf{0} & & \cdots & \mathbf{0} & \mathbf{0} \\ \mathbf{0} & \mathbf{I} & & \cdots & \mathbf{0} & \mathbf{0} \\ \vdots & \vdots & & \ddots & \vdots & \vdots \\ \mathbf{0} & \mathbf{0} & & \cdots & \mathbf{I} & \mathbf{0} \end{bmatrix}, \\ \mathbf{B}_0 &= \begin{bmatrix} \mathbf{b}_0 \\ \mathbf{o} \\ \vdots \\ \mathbf{o} \end{bmatrix}, \ \mathbf{B}_2 = \begin{bmatrix} \mathbf{b}_2 \\ \mathbf{o} \\ \vdots \\ \mathbf{o} \end{bmatrix}, \ \mathbf{B}_\tau = \begin{bmatrix} \tilde{\mathbf{b}}_\tau \\ \mathbf{o} \\ \vdots \\ \mathbf{o} \end{bmatrix}, \ \mathbf{C} = \begin{bmatrix} \mathbf{c} & \mathbf{o}^{\text{T}} & \cdots & \mathbf{o}^{\text{T}} \end{bmatrix}, \end{aligned} \tag{36}$$

cf. (18,19,20). There are $\tau(k) - 2$ zero matrices in the first row of $\mathbf{A}_{\tau(k)}$. Note that the size of $\mathbf{A}_{\tau(k)}$, $\mathbf{B}_0$, $\mathbf{B}_\tau$, $\mathbf{B}_2$, and $\mathbf{C}$ increases with $\tau(k)$. Later we will need to multiply matrices and vectors corresponding to different $\tau(k)$ values, thus they must be augmented to same size. $\mathbf{A}_{\tau(k)}$ can be augmented to the size of $\mathbf{A}_n$ in the following manner:

$$\hat{\mathbf{A}}_{\tau(k)} = \begin{bmatrix} \mathbf{a}_0 & \tilde{\mathbf{a}}_1 & \mathbf{0} & \cdots & \mathbf{0} & \tilde{\mathbf{a}}_\tau & \mathbf{0} & \cdots & \mathbf{0} & \mathbf{0} \\ \mathbf{I} & \mathbf{0} & & & \cdots & & & & \mathbf{0} & \mathbf{0} \\ \mathbf{0} & \mathbf{I} & & & \cdots & & & & \mathbf{0} & \mathbf{0} \\ \vdots & \vdots & & & \ddots & & & & \vdots & \vdots \\ \mathbf{0} & \mathbf{0} & & & \cdots & & & & \mathbf{I} & \mathbf{0} \end{bmatrix}, \tag{37}$$

while $\hat{\mathbf{B}}_0$, $\hat{\mathbf{B}}_\tau$, $\hat{\mathbf{B}}_2$, and $\hat{\mathbf{C}}$ are augmented simply by filling them up with $n - \tau(k)$ zero vectors $\mathbf{o}$ and $\mathbf{o}^{\text{T}}$.

In this work we analyze the cases, where every n-th packet is received periodically. The corresponding effective delay variations are shown in Fig. 3(b), while for the follower's velocity they remain the same as in Fig. 3(a). In order to perform stability analysis, the evolution of the system throughout a whole principal period $T = n\Delta t$ must be considered; see Insperger and Stépán (2011). Assume that the packet is received at $k\Delta t$, then the delay varies linearly from Δt to $(n+1)\Delta t$ in the interval $\big[k\Delta t,\ (k+n)\Delta t\big)$. The corresponding dynamics are described by map (35) with $\tau(k) = 1$, $\tau(k+1) = 2$, …, $\tau(k+n-1) = n$. Thus, using (35) successively in one principal period yields

$$\begin{aligned} X(k+1) = {} & \hat{\mathbf{A}}_1 X(k) \\ & + \hat{\mathbf{B}}_0 u(k) + \hat{\mathbf{B}}_2 u(k-2) + \hat{\mathbf{B}}_\tau u(k-1) \,, \\ X(k+2) = {} & \hat{\mathbf{A}}_2 X(k+1) \\ & + \hat{\mathbf{B}}_0 u(k+1) + \hat{\mathbf{B}}_2 u(k-1) + \hat{\mathbf{B}}_\tau u(k-1) \,, \\ & \vdots \\ X(k+n) = {} & \hat{\mathbf{A}}_n X(k+n-1) \\ & + \hat{\mathbf{B}}_0 u(k+n-1) + \hat{\mathbf{B}}_2 u(k+n-3) + \hat{\mathbf{B}}_\tau u(k-1) \,. \end{aligned} \tag{38}$$

Similar to the plant stability analysis in Section 4, substituting $u(k) = 0$ into (38) gives

$$X(k+1) = \mathbf{A}X(k) \ , \tag{39}$$

where $\mathbf{A} = \prod_{j=1}^{n} \hat{\mathbf{A}}_j$, and all eigenvalues of $\mathbf{A}$ must lie within the unit circle to ensure plant stability. The plant stability boundaries can be obtained similarly to the no packet loss case presented in Sec. 4. For string stability analysis, applying Z-transform to (38) leads to the transfer function

$$\Gamma_n(z) = \mathbf{C}\left(z^n\mathbf{I} - \mathbf{A}\right)^{-1}\mathbf{G}_n(z) \ , \tag{40}$$

where $\mathbf{G}_n(z)$ is given by the recursive rule

$$\begin{aligned}\mathbf{G}_1(z) =& \hat{\mathbf{B}}_0 + \hat{\mathbf{B}}_2 z^{-2} + \hat{\mathbf{B}}_\tau z^{-1} \ , \\ \mathbf{G}_k(z) =& \hat{\mathbf{A}}_k\mathbf{G}_{k-1}(z) + \hat{\mathbf{B}}_0 z^{k-1} + \hat{\mathbf{B}}_2 z^{k-3} + \hat{\mathbf{B}}_\tau z^{-1}\end{aligned} \tag{41}$$

for $k = 1, \ldots, n$. Due to the algebraic complexity of the transfer function (40-41) the string stability boundaries cannot be expressed explicitly. To compute the string stable domain we create a grid in the (β, α)-plane and check at the meshpoints whether $\Gamma_n\left(\mathrm{e}^{\mathrm{i}\omega\Delta t}\right)$ is below 1 for all ω. Fig. 5 (a,b,c) show the stability diagrams in the (β, α)-plane for $n = 2, 3, 4$, using the same color and shading scheme as in Fig. 4. As n increases the stable domains vary significantly and it becomes difficult to find a point in the (β, α)-plane that is stable for all packet loss scenarios.

Again, when the sampling time is above the critical value, the plant and string stable domain disappears. Similar to the no packet loss case, the critical sampling period of the different packet loss scenarios can be obtained analytically by calculating the locations of the intersection points of the string stability curves and finding the sampling period for which these points coincide. The results are summarized in Table 1 for $n = 2, 3, 4$. These give the numerical values $\Delta t_{\text{crit}} = 0.182, 0.157, 0.137$ [s] for $n = 2, 3, 4$, respectively.

Table 1. Critical sampling period when every n-th packet is received.

n	2	3	4
Δt_{crit}	$\frac{0.2857}{V'(h^*)}$	$\frac{0.2471}{V'(h^*)}$	$\frac{0.2146}{V'(h^*)}$

Note that the loss of data packets in the communication decreases the critical sampling period. Hence frequent packet losses may destabilize the system if the applied sampling time is not small enough.

6. APPLICATION OF A PREDICTOR

One way to decrease the detrimental effects of the increasing time delay induced by packet losses is to predict the missing leader's velocity and headway. For the sake of simplicity, we restrict ourselves to predicting the headway only, based on the newest leader's velocity and follower's velocity. According to (1), the headway can be predicted by integrating the velocity difference of the two vehicles, which can be approximated in many different ways. Fig. 6 shows one possible solution. The distance that the follower travels, i.e., the area under $v_{\text{F}}(t)$ is approximated by trapezoids, since the cruise control prescribes a piecewise constant acceleration for the follower, and hence $v_{\text{F}}(t)$ is theoretically piecewise linear. Whereas the distance that

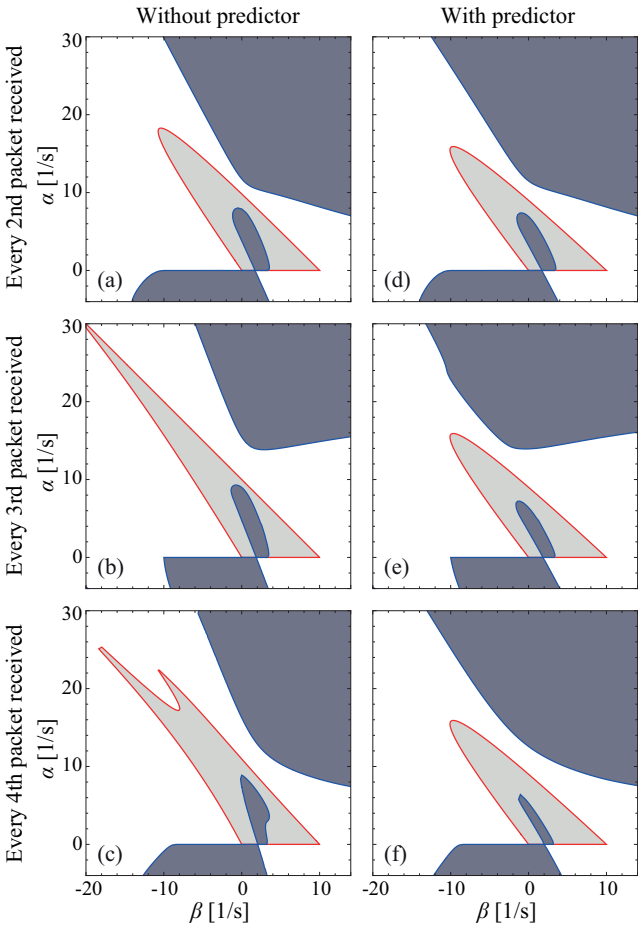

Fig. 5. Stability diagrams of the system subject to packet loss without predictor (left column) and with predictor (right column) in the (β, α)-plane, when every second (first row), every third (second row), and every fourth (third row) packet is received.

the leader travels, i.e., the area under $v_{\text{L}}(t)$ is approximated by rectangles, as newest available leader velocity data is kept constant during packet losses (similarly to the application of a zero-order hold). Henceforth, the corresponding predicted headway becomes

$$\begin{aligned}h_{\text{P}}(t_{k-1}) =& h(t_{k-\tau(k)}) + v_{\text{L}}(t_{k-\tau(k)})(\tau(k)-1)\Delta t \\ &- \sum_{j=1}^{\tau(k)-1} \frac{v_{\text{F}}(t_{k-j-1}) + v_{\text{F}}(t_{k-j})}{2}\Delta t \ ,\end{aligned} \tag{42}$$

where $\tau(k) \geq 2$. Also, no prediction is needed in the no packet loss scenario, since $\tau(k) = 1$ yields $h_{\text{P}}(t_{k-1}) = h(t_{k-1})$.

In the presence of the predictor for the cases investigated in Section 5, the control law becomes

$$\begin{aligned}\dot{v}_{\text{F}}(t) =& \alpha\left[V\left(h_{\text{P}}(t_{k-1})\right) - v_{\text{F}}(t_{k-1})\right] \\ &+ \beta\left[W\left(v_{\text{L}}(t_{k-\tau(k)})\right) - v_{\text{F}}(t_{k-1})\right], \quad t \in [t_k, t_{k+1}),\end{aligned} \tag{43}$$

cf. (32). Solving system (1,43) subject to leader's velocity (12), and linearizing the system yields the discrete-time map

$$\begin{aligned}X(k+1) =& \mathbf{A}^{\text{P}}_{\tau(k)}X(k) \\ &+ \mathbf{B}_0 u(k) + \mathbf{B}^{\text{P}}_{\tau(k)}u\big(k-\tau(k)\big) + \mathbf{B}_2 u(k-2) \ ,\end{aligned} \tag{44}$$

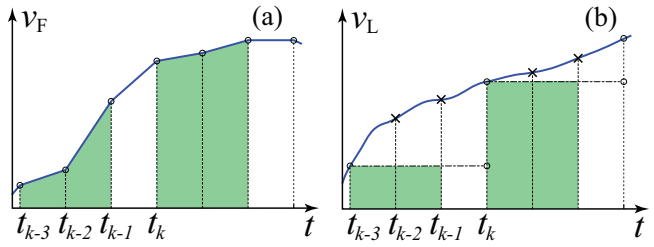

Fig. 6. The areas used for predicting the headway in case of packet loss (when every third packet is received at $..., t_{k-3}, t_k, t_{k+3}, ...$).

where

$$\mathbf{A}^{\mathrm{P}}_{\tau(k)} = \mathbf{A}_{\tau(k)} + \Delta\mathbf{A}_{\tau(k)} \ ,$$
$$\mathbf{B}^{\mathrm{P}}_{\tau(k)} = \mathbf{B}_{\tau} + \Delta\mathbf{B}_{\tau(k)} \ , \qquad (45)$$

and

$$\Delta\mathbf{A}_{\tau(k)} = \begin{bmatrix} \mathbf{0} & \mathbf{a}^{\mathrm{P}}/2 & \mathbf{a}^{\mathrm{P}} & \cdots & \mathbf{a}^{\mathrm{P}} & \mathbf{a}^{\mathrm{P}}/2 \\ \mathbf{0} & \mathbf{0} & & \cdots & & \mathbf{0} \\ \vdots & \vdots & & \ddots & & \vdots \\ \mathbf{0} & \mathbf{0} & & \cdots & & \mathbf{0} \end{bmatrix}, \ \Delta\mathbf{B}_{\tau(k)} = \begin{bmatrix} \mathbf{b}^{\mathrm{P}}_{\tau(k)} \\ \mathbf{o} \\ \vdots \\ \mathbf{o} \end{bmatrix},$$

$$\mathbf{a}^{\mathrm{P}} = \begin{bmatrix} 0 & \frac{1}{2}\alpha V'(h^*)\Delta t^3 \\ 0 & -\alpha V'(h^*)\Delta t^2 \end{bmatrix}, \ \mathbf{b}^{\mathrm{P}}_{\tau(k)} = \begin{bmatrix} -\frac{1}{2}(\tau(k)-1)\alpha V'(h^*)\Delta t^3 \\ (\tau(k)-1)\alpha V'(h^*)\Delta t^2 \end{bmatrix}. \qquad (46)$$

cf. (35,36). The stability analysis in the presence of the predictor can be done in the same way as discussed in Section 5.

Fig. 5 (d,e,f) show the stability diagrams with predictor, where every second, third, and fourth packet is received, respectively. Without predictor (left column), the plant stable domains vary significantly for the different packet loss scenarios. However, with predictor (right column) these domains remain exactly the same as for no packet loss (cf. Fig. 4), implying that plant stability can be preserved by implementing predictors on headway. This is reasonable since the headway is the only information that needs to be predicted for plant stability in the absence of fluctuation in the leader's velocity. Nonetheless, only predicting the headway does not improve string stability as shown in Fig. 5, which is mainly because string stability is a kind of input-output stability and information of the input is lacking in case of packet loss. Also, there is a causality between headway and velocity difference, i.e., the headway is the aggregation of velocity difference. Predicting the effects does not reveal too much information about the cause. Therefore, we conjecture that if the leader's velocity can be predicted appropriately, e.g. by a first-order hold or utilizing acceleration data, the string stability can also be preserved to a certain extent in case of packet loss.

7. CONCLUSIONS

Connected cruise control with packet drops was analyzed in this paper. We investigated the plant stability and the string stability of a PV controller and presented our results using stability diagrams. We showed that packet drops may influence stability negatively but predictors may be used to maintain the robustness of the design. Future research includes the application of the predictors in case of stochastic packet drop scenarios.

ACKNOWLEDGEMENTS

This work was supported by NSF grant 1300319 and by the Hungarian National Science Foundation under grant OTKA-K105433.

REFERENCES

Caveney, D. (2010). Cooperative vehicular safety applications. *IEEE Control Systems Magazine*, 30, 38–53.

Ge, J.I. and Orosz, G. (2014). Dynamics of connected vehicle systems with delayed acceleration feedback. *Transportation Research Part C*, 46, 46–64.

Insperger, T. and Stépán, G. (2011). *Semi-discretization for time-delay systems*. Springer.

Öncü, S., Ploeg, J., van de Wouw, N., and Nijmeijer, H. (2014). Cooperative adaptive cruise control: Network-aware analysis of string stability. *IEEE Transactions on Intelligent Transportation Systems*, 15(4), 1527–1537.

Orosz, G. (2014). Connected cruise control: modeling, delay effects, and nonlinear behavior. *Vehicle System Dynamics*, p. submitted.

Orosz, G., Wilson, R.E., and Stépán, G. (2010). Traffic jams: dynamics and control. *Philosophical Transactions of the Royal Society A*, 368(1928), 4455–4479.

Qin, W.B., Gomez, M.M., and Orosz, G. (2014). Stability analysis of connected cruise control with stochastic delays. In *the American Control Conference*, 4624–4629.

Qin, W.B., Gomez, M.M., and Orosz, G. (2015). Moment-based plant and string stability analysis of connected cruise control with stochastic delays. In *the American Control Conference*, accepted.

Qin, W.B. and Orosz, G. (2013). Digital effects and delays in connected vehicles: linear stability and simulations. In *the ASME Dynamic Systems and Control Conference*, DSCC2013-3830, V002T30A001.

Rajamani, R. and Shladover, S. (2001). An experimental comparative study of autonomous and co-operative vehicle-follower control systems. *Transportation Research Part C: Emerging Technologies*, 9(1), 15–31.

Stépán, G. (2001). Vibrations of machines subjected to digital force control. *International Journal of Solids and Structures*, 38(10–13), 2149–2159.

Swaroop, D. and Hedrick, J.K. (1996). String stability of interconnected systems. *IEEE Transactions on Automatic Control*, 41(3), 349–357.

van Arem, B., van Driel, C., and Visser, R. (2006). The impact of cooperative adaptive cruise control on traffic-flow characteristics. *IEEE Transactions on Intelligent Transportation Systems*, 7(4), 429–436.

Verriest, E.I. and Michiels, W. (2009). Stability analysis of systems with stochastically varying delays. *Systems and Control Letters*, 58, 783–791.

Zhang, L. and Orosz, G. (2015). Motif-based analysis of connected vehicle systems: delay effects and stability. *IEEE Transactions on Intelligent Transportation Systems*, p. submitted.